Steady and oscillatory applied sheared flows in global gyrokinetic simulations

N. Ohana[1], L. Villard[1], E. Lanti[1], S. Brunner[1], B. F. McMillan[2], N. Tronko[3], A. Bottino[3], A. Biancalani[3], I. Novikau[3], A. Mishchenko[4]

[1] *École Polytechnique Fédérale de Lausanne (EPFL), Swiss Plasma Center (SPC), CH-1015 Lausanne, Switzerland*

[2] *Centre for Fusion, Space and Astrophysics, Department of Physics, Warwick University, Coventry, UK*

[3] *Max Planck Institute for Plasma Physics, Garching, Germany*

[4] *Max Planck Institute for Plasma Physics, Greifswald, Germany*

Introduction

In order to get a better understanding of the linear and nonlinear interaction of microinstabilities and associated turbulence with different specific modes, an ad-hoc "antenna" is implemented in the global electromagnetic gyrokinetic PIC code ORB5 [1, 2]. It consists in applying time-dependent external charge- and current-density perturbations or, alternatively, external electrostatic and magnetic potentials, to the system. The fields created by the antenna are considered separately from the fields of the plasma response and can thus be accounted for even in linear simulations where the perturbed self-consistent plasma field contributions to the particle orbits are neglected.

(De-)stabilization of linear ITG modes by steady and oscillatory applied sheared flows

In a first step, the antenna is used to excite zonal structures in a Cyclone-base case (ITG, adiabatic electrons). Simulation parameters are taken from [3]. Without antenna, the linear growth rate of the ITG mode with toroidal mode number $n = 20$ (corresponding to $k_\theta \rho = 0.3$) is $\gamma = 8.12 \cdot 10^{-2}\ c_{s0}/a$, where c_{s0} is the sound velocity at a reference surface and a the plasma minor radius. The ad-hoc antenna radial profile is chosen such that the associated shearing rate is $\omega_{E\times B}(s) = \omega_{E\times B}(s_0)\, s/s_0$, where s is the radial coordinate defined as $\sqrt{\psi/\psi_{\text{edge}}}$, ψ being the poloidal flux, and s_0 is a reference surface. To begin with, the antenna field is constant in time.

Figure 1 shows the effect of the applied sheared flow on the mode growth rate. A total stabilization is achieved when $\omega_{E\times B} \gtrsim 3 \cdot 10^{-2}\ c_{s0}/a$, which is comparable to the linear growth rate without antenna. The growth rate is maximal for $\omega_{E\times B}(s_0) = \omega_{E\times B,0} := -8.5 \cdot 10^{-3}\ c_{s0}/a$, when antenna shearing rate compensates the $\omega^\star$ shearing effect, as shown in [4].

A sinusoidal time dependence is then added to the shearing rate, with a frequency ω_{ant} and an amplitude $\Delta\omega_{E\times B} = 9 \cdot 10^{-3}\ c_{s0}/a$ around the steady value $\omega_{E\times B,0}$.

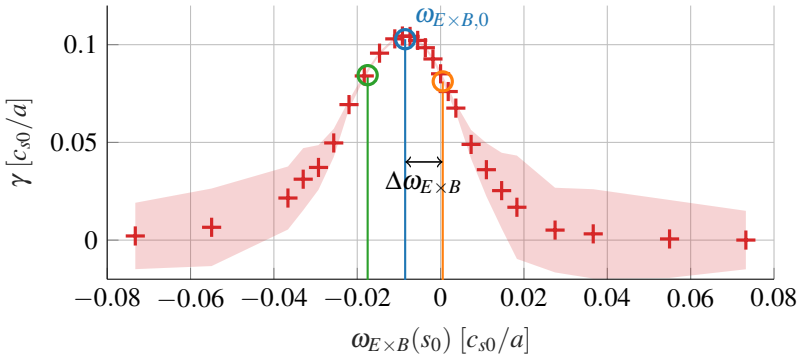

Figure 1: Time-averaged linear growth rate of ITG mode with toroidal mode number $n = 20$ as a function of antenna's steady shearing rate. Colored area height is plus or minus the standard deviation of the instantaneous growth rate. Circles indicate references for upcoming Figure 2.

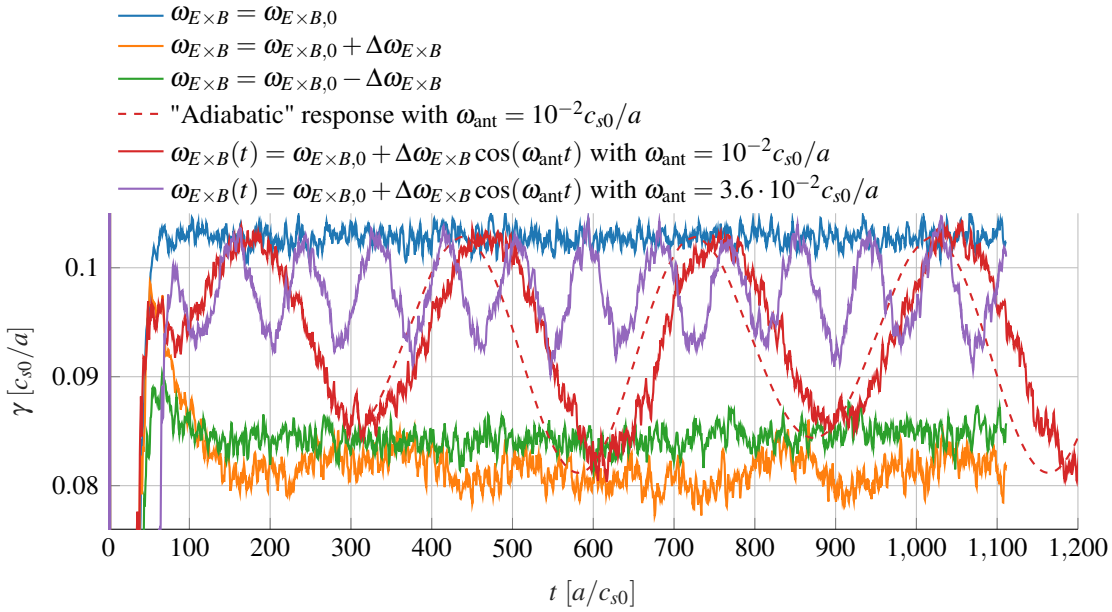

Figure 2: Instantaneous growth rate as a function of time for stationary and oscillatory applied sheared flows. The so-called "adiabatic" response is the growth rate corresponding to the instantaneous antenna shearing rate in the limit of steady sheared flows, interpolated from Figure 1 data.

Time traces of the instantaneous growth rate of the mode in presence of oscillatory sheared flows are depicted in Figure 2. For a low frequency $\omega_{\text{ant}} = 10^{-2}\ c_{s0}/a$, the instantaneous growth rate oscillates closely following the "adiabatic" response with a small time lag. For a higher frequency $\omega_{\text{ant}} = 3.6\cdot 10^{-2}\ c_{s0}/a$, corresponding oscillations have a weaker amplitude and the average growth rate gets closer to the one with a steady applied flow $\omega_{E\times B,0}$ only.

This behavior is further analyzed in Figure 3 by computing the effective shearing rate $\omega_{E\times B,\text{eff}}$, meaning the static shearing rate corresponding to the average growth rate, as a function of ω_{ant}. In other words, $\omega_{E\times B,\text{eff}}$ satisfies $\gamma(\omega_{E\times B,0} + \omega_{E\times B,\text{eff}}) = \bar{\gamma}(\omega_{\text{ant}})$ where $\bar{\cdot}$ stands for the time average. For a given ω_{ant}, two solutions are interpolated from Figure 1's $\gamma(\omega_{E\times B})$ data. Results show a good agreement with previous analytical work [5], using an equivalent turbulence decorrelation time $\Delta\omega_T = 6.3\cdot 10^{-3} c_{s0}/a$ (providing best fit).

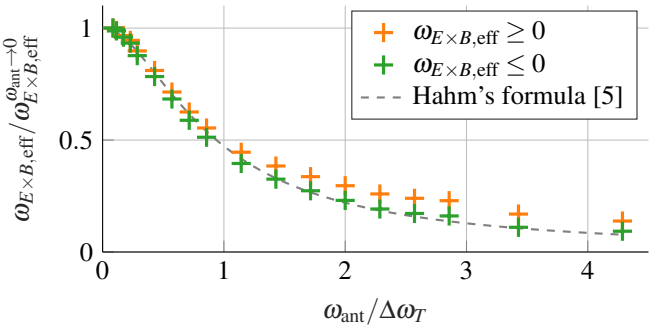

Figure 3: Effective shearing rate as a function of the antenna oscillation frequency. Turbulence decorrelation time $\Delta\omega_T$ in Hahm's formula [5] has been set to $6.3\cdot 10^{-3} c_{s0}/a$ providing best fit with simulation results.

Non-linear TEM with self-consistent and applied zonal flows

As a second application, the nonlinear plasma response is included to study the effectiveness of the turbulence saturation by sheared flows. In a case of TEM-dominated system, chosen with electron to ion temperature at reference surface $T_{e0}/T_{i0} = 1$, electron temperature logarithmic gradient $R/L_{Te} = 7$, and electron and ion stability factors $\eta_e = 3$ and $\eta_i = 1$. Detailed parameters can be found in [1]. ORB5's hybrid electron model [2] is used. For these parameters, the effect of zonal flows on transport is significant, in agreement with [6]. Indeed, as depicted in Figure 4, the quasisteady electron heat diffusivity is about 3 times higher when self-consistent zonal flows are filtered out from the simulation than when they are included.

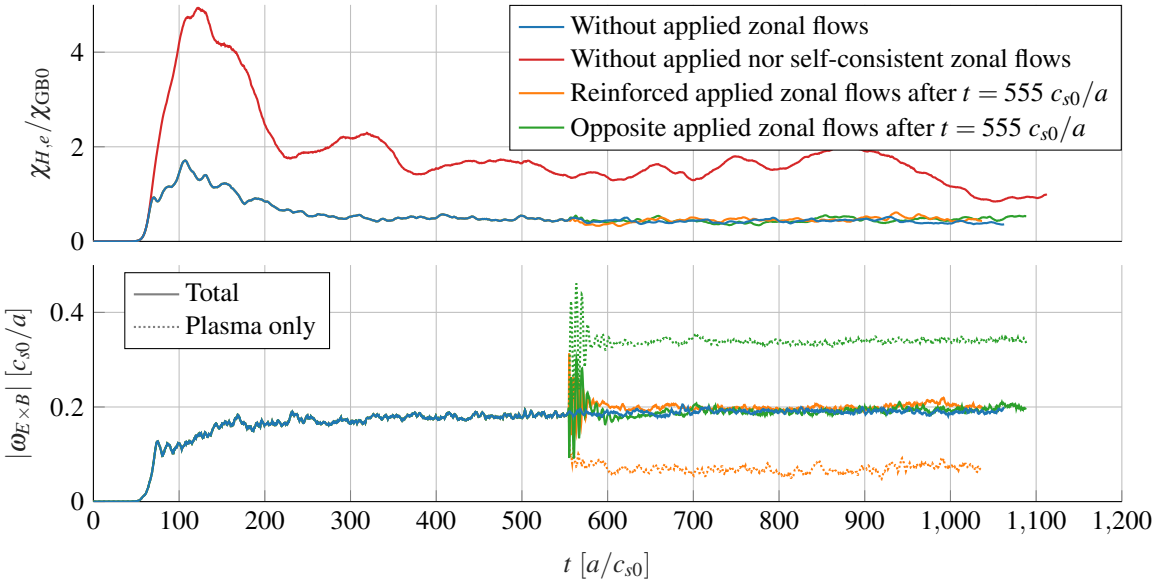

Figure 4: Temporal evolution of the electron heat diffusivity $\chi_{H,e}$ and shearing rate averaged from $\rho_{\mathrm{vol}} = 0.3$ to $\rho_{\mathrm{vol}} = 0.7$.

After $t = 555\ c_{s0}/a$, steady zonal flows are applied by the antenna. Their profile is chosen as the time-averaged self-consistent zonal flows from $t = 278\ c_{s0}/a$ to $t = 555\ c_{s0}/a$. The self-consistent zonal flow amplitude is observed to decrease so that the total (self-consistent and applied) zonal flows regain their previous level after a transient phase (orange curves in Figure

4). As a consequence, the heat diffusivity is not affected by the applied zonal flows. The same behavior appears when the opposite zonal flow profile is applied after $t = 555\ c_{s0}/a$ (green curves in Figure 4), but this time the plasma zonal flow level is doubled after a transient phase so that total quasisteady zonal flows and heat diffusivity are unchanged.

Linear GAM excitation

The antenna has also been used to address the question of the origin of nonlinear zonal structures (avalanche-like features) observed to propagate in the TCV tokamak at a frequency similar to the one of local GAMs at the edge. Those structures have been experimentally observed in [7], and numerically reproduced in [8, 9]. Even though we managed to linearly excite GAMs with the antenna, they were not found to propagate below the local GAM frequency [10], unlike the avalanche-like features observed in nonlinear simulations.

Conclusion

First, linear studies have shown the effectiveness of stationary and oscillatory sheared flows to stabilize or destabilize ITG modes. Second, the heat transport has been found to be unaffected by applied stationary $E \times B$ flows, because plasma self-consistent zonal flows reorganise themselves to compensate the applied ones. Finally, linear GAM excitation revealed that the global coherent mode propagating in TCV cannot be explained by linear theory alone. Future work will include plasma turbulence in those simulation to see if it can act as a support for the avalanche propagation.

Acknowledgments

This work has been carried out within the framework of the EUROfusion Consortium and has received funding from the Euratom research and training programme 2014-2018 and 2019-2020 under grant agreement No 633053. The views and opinions expressed herein do not necessarily reflect those of the European Commission. Simulations were performed on the Piz Daint GPU platform at CSCS.

References

[1] S. Jolliet et. al., Comput. Phys. Com., **177**(5), 409-425, 2007

[2] E. Lanti et. al., Comput. Phys. Com., submitted

[3] T. Görler et. al., Phys. Pl., **23**(7), 072503, 2016

[4] N. Ohana et. al., Journ. Phys. Conf. Series, **11125**(1), 012017, 2018

[5] T.S. Hahm et. al., Phys. Pl., **6**(3), 922-926, 1999

[6] J. Lang et. al., Phys. Pl., **15**(5), 055907, 2008

[7] Z. Huang et. al., Pl. Phys. Contr. Fus., **60**(3), 034007, 2018

[8] G. Merlo et. al., Pl. Phys. Contr. Fus., **60**(3), 034003, 2018

[9] L. Villard et. al., Pl. Phys. Contr. Fus., **61**(3), 034003, 2019

[10] Z. Gao, Phys. Pl., **17**(9), 092503, 2010